Pergamon

Int. J. Solids Structures Vol. 33, No. 10, pp. 1479–1500, 1996

0020-7683/96 $15.00 + .00

0020-7683(95)00105-0

ON THE LARGE DEFORMATION AND LOCALIZATION BEHAVIOR OF AN EPOXY RESIN UNDER MULTIAXIAL STRESS STATES

Y.-M. LIANG and K. M. LIECHTI

Engineering Mechanics Research Laboratory, Department of Aerospace Engineering and Engineering Mechanics, The University of Texas at Austin, Austin, TX 78712, U.S.A.

(*Received* 7 *June* 1994; *in revised form* 17 *April* 1995)

Abstract—The paper describes a series of experiments that were conducted in order to examine the response of a cross linked epoxy resin. A variety of stress states were considered by conducting experiments under uniaxial tension, plane strain compression, simple shear and combinations of tension or compression and shear (biaxial). Strain rate effects were considered in the simple shear experiments and displacement measurements using geometric moiré were made in order to follow the onset and propagation of shear bands under simple shear and compression on shear. Some birefringence measurements were also made.

Localization in the form of shear bands occurred under the tensile, simple shear and the biaxial stress states but not under plane strain compression. The shear bands in simple shear and compression and shear grew quickly along the specimen gage length and then broadened, and detailed strain distributions were determined as a function of load level. The birefringence became constant in regions where shear banding had occurred. The onset of shear banding was delayed by higher strain rates and compressive stresses but was promoted by tensile stresses. The lack of a limit load in the plane strain compression response indicates that the epoxy considered here does not strain soften and that the response obtained is the true material one.

1. INTRODUCTION

The motivation for examining the formation of shear banding in the crosslinked epoxy resin being considered here was that it had been observed during interfacial crack initiation and propagation in glass/epoxy blister specimens (Liechti and Liang, 1992). Optical interference measurements of normal crack opening displacements indicated that shear bands emanated from undulations in the crack front. The degree of dissipation and toughening provided by shear banding is required in order to assess the extent of toughening that has been observed under various conditions (Liang and Liechti, 1995).

Although shear banding is commonly associated with thermoplastic polymers [see the review by G'Sell (1986)] where the lack of crosslinking provides sufficient mobility for molecular chains, a number of observations have been made of localization in thermosetting polymers. These observations have, of course, been made in specimens under compressive or shear loadings where crack initiation can be suppressed to a certain degree. In the work on yielding in uniaxial compression (Yamini and Young, 1980; Lee, 1988), yielding in these studies was taken to be the flattening of or a maximum in the compressive stress/strain response. The mechanism of yielding was associated on the microscopic level with molecular chain kinking (Argon and Bessonov, 1977) or disc-shaped regions of shearing (Bowden and Jukes, 1972). These associations were made on the basis of the strain rate and/or the temperature dependence of yielding that are predicted by the theories of Argon and Bowden (originally developed for thermoplastics), rather than by direct observations of localizations on any level. Lee (1988) points out that the crosslinks in thermosets do not interfere with the activation of molecular kinking, although they do indirectly affect the yield strength itself by virtue of their influence on chain packing. A more direct association of mechanisms on the microscopic and macroscopic scales has come from the work of G'Sell *et al.* (1990) that involved the simple shearing of cyanate and epoxy-based resins. From local shear strain measurements, it was found that a single shear band grew in the specimen and that

the response of the materials in shear was very similar to that of thermoplastics, except that the strain range was smaller.

The Argon model (1973) was generalized into a three dimensional constitutive relation with strain softening by Boyce *et al.* (1988) and further modified in the final strain hardening regime by Arruda and Boyce (1993a), using their three dimensional rubber elasticity model (1993b). These and further modifications (Wu and van der Giessen, 1992) for the strain hardening regime were used to predict (Boyce *et al.* 1992; Wu and van der Giessen, 1993) the formation of shear banding in the polycarbonate shear experiments that were reviewed by G'Sell (1986). The predictions were able to capture the onset and propagation of a shear band. It was found (Wu and van der Giessen, 1993) that predictions of the accompanying normal stresses were higher than measured values. The experiments and data generated in this study can be expected to provide the basis for similar analyses.

In the work reported here, a series of experiments was conducted in order to examine the mechanical behavior of the epoxy. These included tests in tension, plane strain compression and biaxial tests with tension or compression on shear. The paper describes the procedures that were used, the observations that were made and the parameters that were extracted for modeling.

2. EXPERIMENTAL PROCEDURES

This section describes the experimental procedures that were used to characterize the deformation response of a bisphenol A epoxy with an amido amine hardener† under a variety of stress states. Constant displacement and, in some cases, constant strain rate experiments were conducted in tension, plane strain compression, pure shear, shear with tension and shear with compression.

2.1. *Uniaxial tension*

Uniaxial tension tests were conducted on epoxy specimens which had the geometry shown in Fig. 1(a). A nominal strain rate of $0.5 \times 10^{-3}\ s^{-1}$ was applied to the specimen with a servohydraulic machine. The load was measured by a load cell with a maximum capacity of 98 kN, and the longitudinal and transverse strains were measured by a strain gage (EP-08-125TA-120) with maximum range of 10%. The stress–strain response is shown in Fig. 2. The response was matched up to 3% strain by a Ramberg–Osgood fit:

$$\varepsilon = \frac{\sigma}{E} + \bar{\alpha}\left(\frac{\sigma}{\sigma_0}\right)^{n-1}\frac{\sigma}{E} \tag{1}$$

as a common analytical representation of elastoplastic deformation. The yield offset $\bar{\alpha}$, the hardening exponent n, and the yield stress σ_0, were determined by fitting the test data up to the maximum stress. The initial tangent modulus was 2.03 GPa and the Poisson's ratio $\nu = 0.36$. The response exhibited a maximum due to the onset of a necking localization. The specimens failed shortly after the initiation of necking by fast fracture from a microscopic flaw at about 7% strain.

2.2. *Plane strain compression*

In the tension tests on the epoxy, the engineering stress reached a maximum value when a localization initiated in the specimen. The subsequent load drop associated with necking and propagation was interrupted by fast fracture. Uniaxial compression tests can be used to avoid fast fracture but may still suffer from buckling of the specimens. This potential disadvantage was overcome in the plane strain compression test proposed for polymers by Ford *et al.* (1952). A sheet of material is placed between two parallel, flat and highly polished steel bars [Fig. 1(b)]. If the steel bars are lubricated, friction can be neglected (Williams and Ford, 1964) and the bars provide no constraint to elongation in the x- and z-directions. The test has the advantage that the area under load remains constant and no

†We are grateful to Ciba Geigy for supplying Araldite 502 epoxy resin and HY955 hardener.

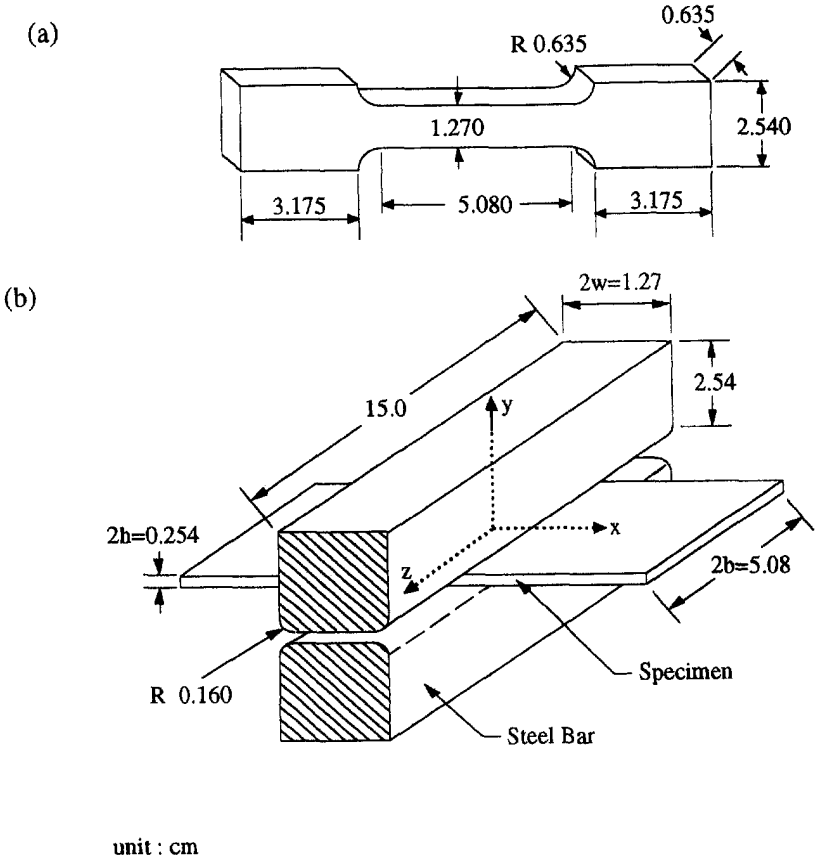

Fig. 1. Specimen geometry for (a) uniaxial tension test (b) plane strain compression test.

instability due to reduction in area ("geometric effect") can occur. In contrast to the tension test, the compressive stress calculated by dividing the force by the area is the Cauchy stress.

A stiff, electromechanical loading device with ground plattens was used to apply the compressive loads under ramped crosshead position control at a nominal strain rate of $1.25 \times 10^{-3}\ s^{-1}$, which was more than double the rate used in the uniaxial tension test but was the lowest rate available. The load was measured by a load cell with a maximum

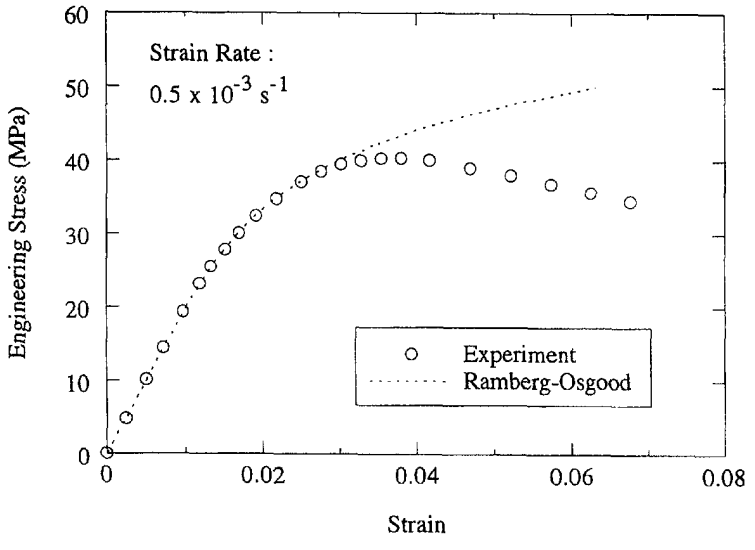

Fig. 2. Stress–strain response of uniaxial tension test.

capacity of 196 kN. To ensure uniformity of the applied pressure on the specimen, a height gauge with 12 μm precision was used to check the alignment of the plattens. In addition, two spring-loaded LVDTs, placed at the ends of the steel bars, were used to measure their relative movement. The alignment of the plattens during loading was easily confirmed from the LVDT measurements. Due to the compliance of the steel bars, the strain in the epoxy was determined from

$$\varepsilon_{\text{epoxy}} = \frac{2\Delta_y}{L_e}\left(1 + \frac{E_e L_s}{E_s L_e}\right)^{-1} \tag{2}$$

where $2\Delta_y$ is the applied displacement, $L_e = 2h$ is the height of the epoxy, E_s and E_e are Young's moduli of the steel bar and epoxy, and L_s is the total height of the steel bars that was spanned by the displacement transducer.

The corners of the steel bars were rounded to a radius of 0.16 cm to reduce the stress concentrations which might cut into the epoxy during the experiment. In addition, the surfaces on which the loads were applied had to be smooth to allow the materials to slide easily. Rough surfaces restrain the sliding and complicate the stress state in the epoxy. An estimate of the stress state in the epoxy between the bars can be obtained (Williams and Ford, 1964) by assuming $\varepsilon_z = 0$ due to the constraint in the z direction provided by the material outside the punch, and $\sigma_x = 0$ due to frictionless contact between the epoxy and steel bars. As a result, the strains before yielding are simply

$$\varepsilon_y = \frac{1-\nu^2}{E}\sigma_y \quad \text{and} \quad \varepsilon_x = -\frac{\nu(1+\nu)}{E}\sigma_y. \tag{3}$$

Three dimensional finite element analyses (Fig. 3) were conducted to examine the validity of the assumptions used in obtaining eqn (3). Instead of being zero, the normal strain ε_z was about 21% of the applied strain, making the plane strain approximation questionable. In addition, ε_x was about 41% of the applied strain instead of 56% based on eqn (3) and the Poisson's ratio obtained from uniaxial tension tests. The stresses σ_x and σ_z [Fig. 3(b)] were 5.2% and 17% of σ_y for $z/b < 0.6$, which in turn gave rise to $\varepsilon_y = 0.92\sigma_y/E$, which, for the true plane strain conditions (3), should have been $0.87\sigma_y/E$. Thus the relaxation of the plane strain condition resulted in a 5.4% lower slope in the σ_y vs ε_y response.

A simple modification to the steel bar was considered with a view to improving the uniformity of the stress distribution by improving the constraint in the z-direction. The way this was done was to consider machining away a portion ($2b \times h/2$) from each steel bar so that the epoxy width ($2b$) would fit snugly into the bars. The bars were then considered to apply the constraint $u_z = 0$ for $|y| \geqslant h/2$ along $z = \pm b$ [Fig. 1(b)]. The results of this modification are shown in Fig. 4, where it can be seen that the plane strain solution is recovered very well.

The effect of a rounded corner [$R = 0.16$ cm, Fig. 1(b)] was assessed by comparing the stress distributions with those resulting from a sharp corner ($R = 0$). Three through-thickness locations, $y/h = 0$, 0.5, and 1, are shown in Figs 5(a–c). The rounded corner indeed improves the uniformity of the stress distributions in both the x- and y-directions, especially along $y/h = 1$ under the steel bar [Fig. 5(c)], where the assumption $\sigma_x = 0$ is quite reasonable. In Figs 5(a–c), the normal stress $|\sigma_y|$ was 82% of the nominal stress (P/A), where $A = 1.27 \times 5.08$ cm^2. Consequently, the measured nominal stress in any experiment was scaled by 82% in order to obtain the actual stress.

In retrospect, a much simpler approach to conducting truly plain strain compression tests comes from the work of Boyce and Arruda (1992) and Arruda and Boyce (1993a,c), which came to our attention only recently and certainly long after our plane strain compression tests had been conducted.

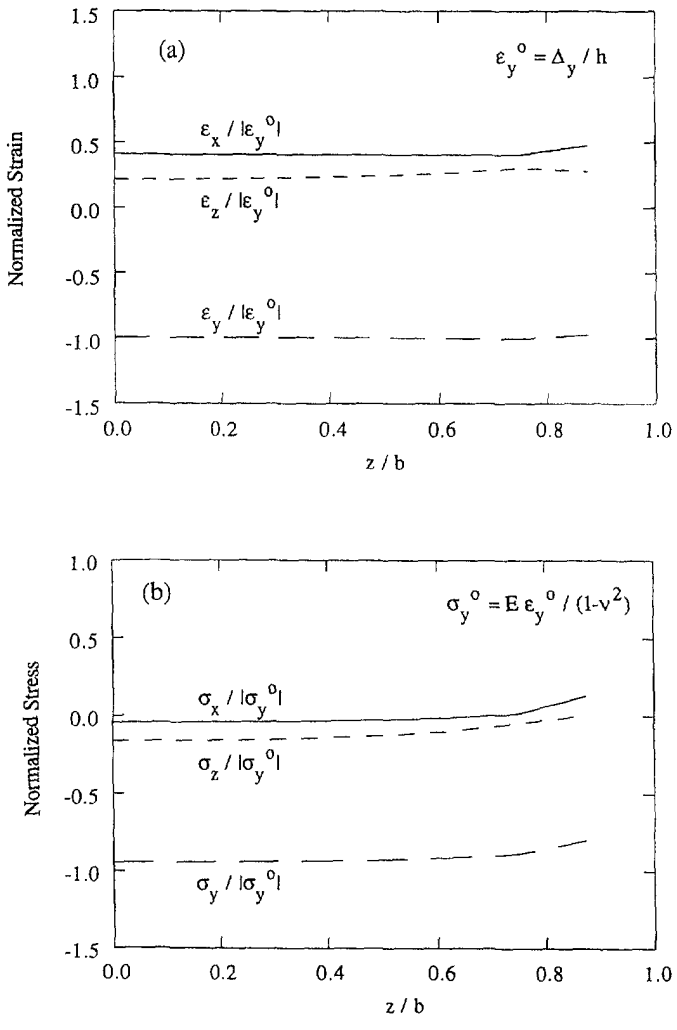

Fig. 3. Strain and stress distributions in the compression test specimen.

2.3. *Combined and simple shear*

The modified Arcan configuration (Arcan *et al.*, 1984) was used to study the epoxy deformation behavior under multiaxial stress states. This test can be used to apply various combinations of tension or compression on shear. The approach that was taken was to measure local deformation in addition to the usual measurements of overall load and grip displacement. The measurements of local deformation were made using geometric moiré in conjunction with digital image processing techniques. Some birefringence measurements were also made.

In the modified Arcan test, a butterfly-shaped specimen was adopted to study material behavior under multiaxial stress states (Fig. 6). The grips and specimen assembly are connected to a simple uniaxial loading device. A range of biaxial stress states was provided by applying tensile loads to any of the diametrically opposed holes in the grip. For a loading angle α counter-clockwise from the y-axis, the stress state in the gage section is given by

$$\sigma_x = (P/A)\sin\alpha, \quad \sigma_y = \nu\sigma_x, \quad \tau_{xy} = -(P/A)\cos\alpha, \tag{4}$$

and $\sigma_z = \tau_{xz} = \tau_{yz}$. The uniformity of the stresses was checked in a linearly elastic finite element analysis that assumed that there was perfect adhesion between the specimen and the grips. The stress distributions along the x- and y-axes are shown in Figs 7(a,b). Along the x-axis, the σ_x and τ_{xy} reach maximum at $x = 0$. The maximum shear stress was about

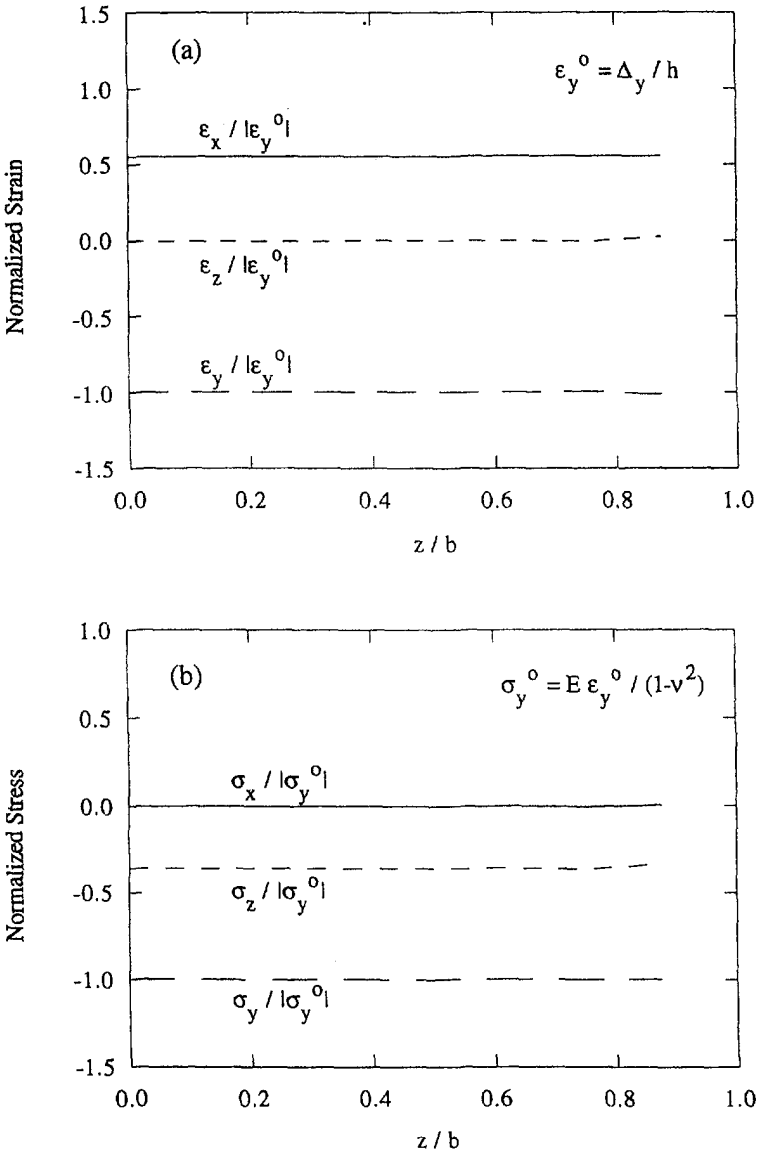

Fig. 4. Strain and stress distributions in the plane strain compression test specimen.

4% lower than the nominal value obtained from static equilibrium. Along the y-axis, the normal stresses reached maximum values at $y = 0$; the shear stress achieved maximum values at $y/L = \pm 0.75$, and inside this region the variations of stresses were relatively small, never exceeding 8% of the nominal value. Although severe stress concentrations have clearly been avoided, the stress gradients, particularly in the y-direction, provide a degree of geometric imperfection that naturally triggered a shear band without any additional measures, such as the one taken by G'Sell (1986).

The Arcan tests were conducted using a servohydraulic, uniaxial loading device running under displacement control. The resulting load, P, was recorded and plotted as a function of the applied displacement, Δ. These parameters were considered to be the global quantities and were supplemented by measurements of the local in-plane displacements in the gage section of the specimen. These measurements were made using a geometric moiré technique that employed a crossed grating. The apparatus used for the global and local displacement measurements is shown schematically in Fig. 8. For the moiré measurements, the specimen was illuminated by transmitted light and was viewed through a low power microscope. The deformed grid was recorded on a video system and was analyzed using a digital image

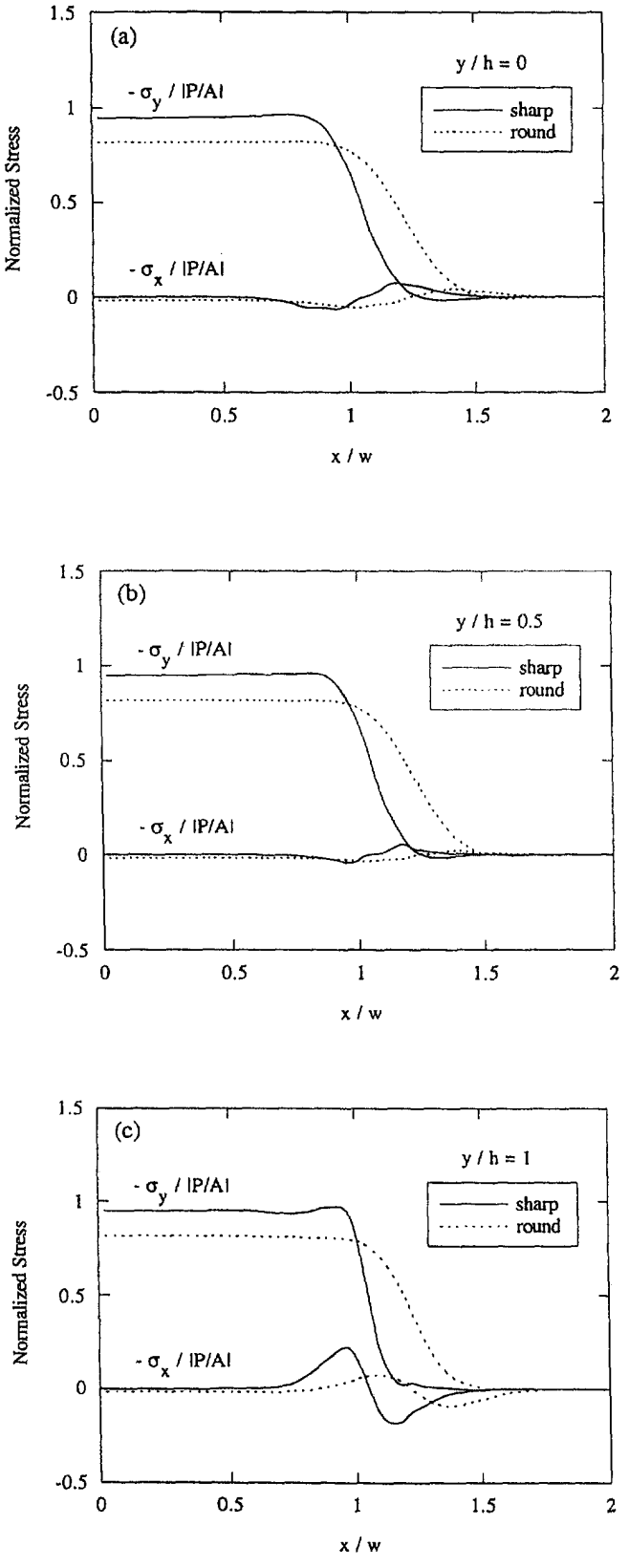

Fig. 5. The effect of pinch radius on the stress distributions in the plane strain compression test specimen.

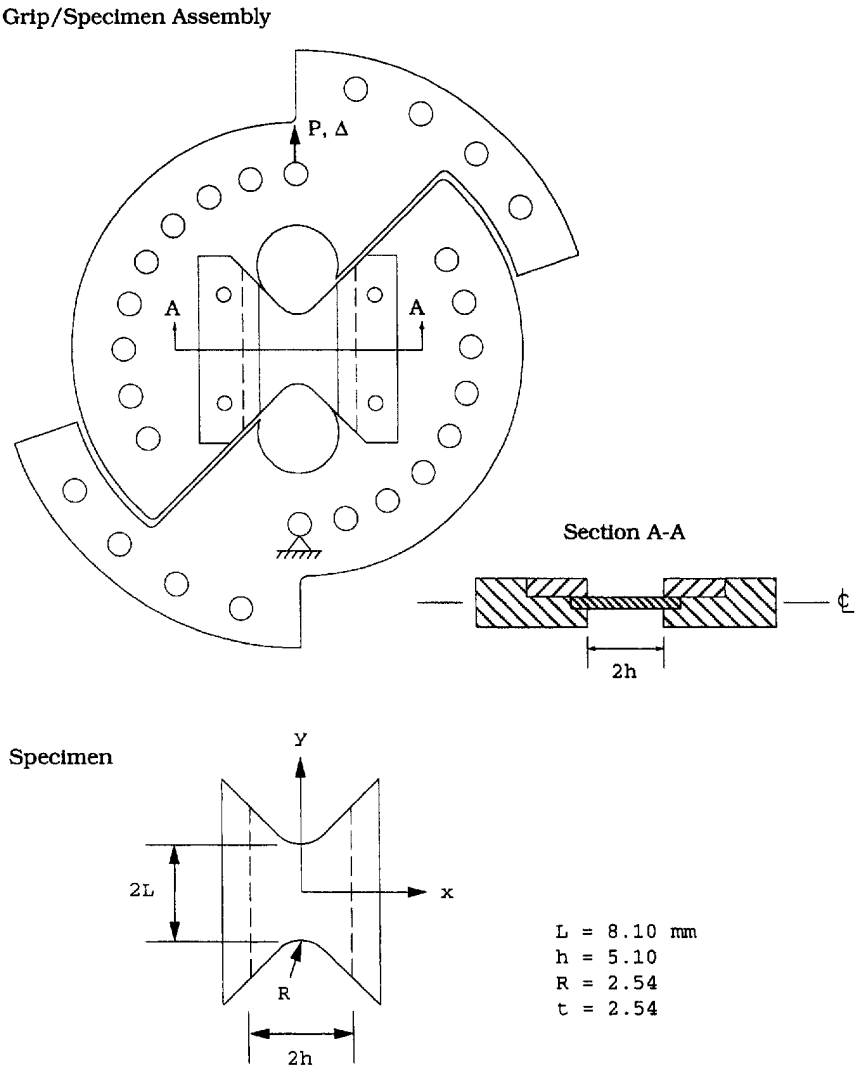

Fig. 6. Arcan test specimen and grips.

analyzer. Using image overlap and filtering processes, the displacement fields were obtained by digitally superposing the deformed grid with the undeformed one. As a result, the in-plane displacements, u and v, can be calculated from

$$u = mp \quad \text{and} \quad v = np \tag{5}$$

where m and n are the moiré fringe orders associated with u and v displacements, and $p = 0.25$ mm was the pitch of the grid. A series of experiments was conducted at various strain rates and ratios of tension or compression to shear.

To further understand the epoxy behavior, an initial photoelastic analysis was also used to estimate the stresses during loading. A two-dimensional photoelastic apparatus was incorporated to generate isochromatic fringe patterns which were recorded by the video system, while the load was measured by using a 2 kN load cell. Treloar (1958) showed that the difference in indices of refraction, n_1 and n_2, was related to the principal stretches, λ_1 and λ_2, through

$$n_1 - n_2 = C(\lambda_1^2 - \lambda_2^2) \tag{6}$$

where the constant C is related to the number of chains per unit volume and the polarizability anisotropy of a repeat unit (Raha and Bowden, 1972). Since, for rubber elasticity,

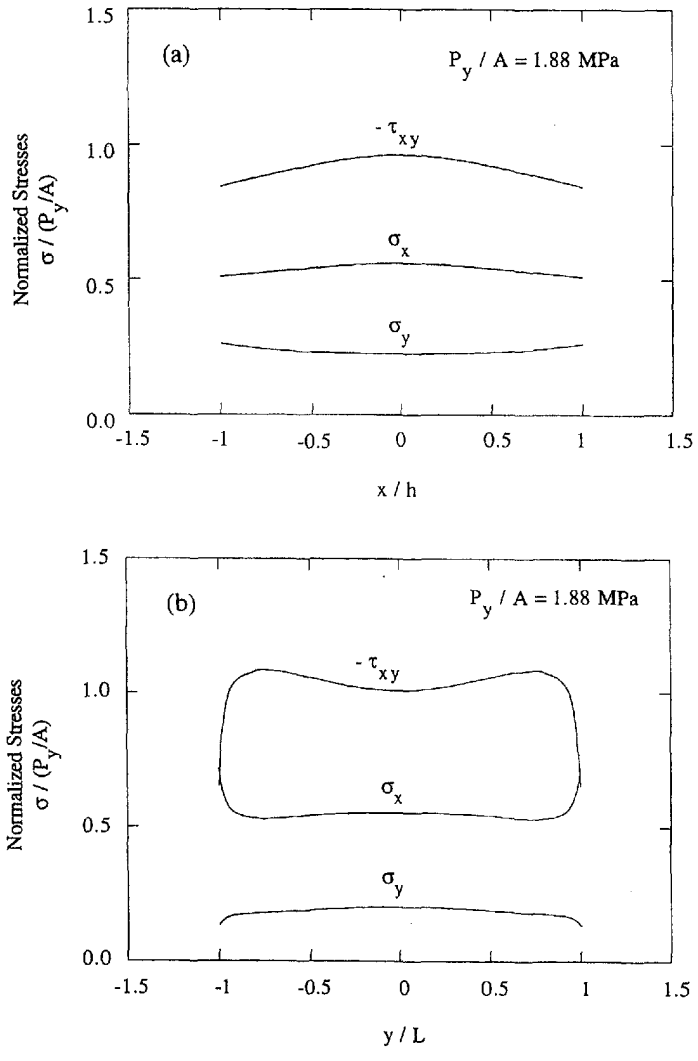

Fig. 7. Stress distributions in an Arcan specimen with $\alpha = 30^\circ$ along (a) the x-axis (b) the y-axis.

the dependence of the difference in principal stresses on the principal stretches has a similar form, the difference in indices of refraction are directly proportional to the difference in principal stresses. In the photoelasticity literature, this has led to the stress–optic law for photoelastic materials, which has the following form

$$N = \frac{h}{f_\sigma}(\sigma_1 - \sigma_2) \tag{7}$$

where σ_1 and σ_2 are the in-plane principal stresses, h is the thickness, and f_σ is the so-called material fringe value which is a material property for a given light wavelength. However, if the material deforms beyond its elastic limit, the relative retardation N will be affected by the inelastic strain. As suggested by Coker and Filon (1957), and further pursued by Buisson and Ravi-Chandar (1990), the stress–optic law (7) should include a term that accounts for the plastic strain, that is

$$N = \frac{h}{f_\sigma}(\sigma_1 - \sigma_2) + \frac{h}{f_\varepsilon}(\varepsilon_1^p - \varepsilon_2^p) \tag{8}$$

where ε_1^p and ε_2^p are the principal plastic strains, and f_ε is the material fringe value due to

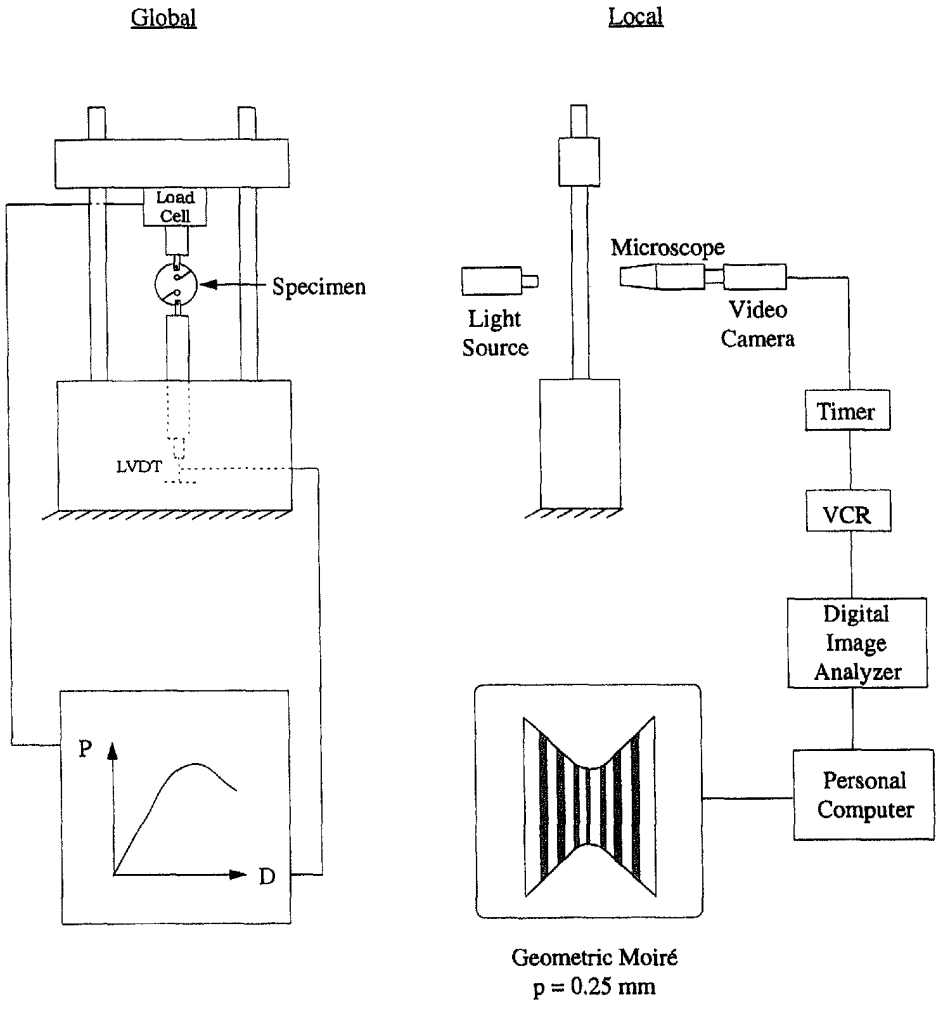

Fig. 8. Schematics of global and local displacement measurements in Arcan test.

the plastic strains. The parameter f_σ can be directly determined from load measurements in photoelastic experiments under pure shear. The parameter f_ε was determined in conjunction with the moiré measurements, where $(\varepsilon_1^p - \varepsilon_2^p)$ was determined directly.

3. RESULTS AND DISCUSSION

The results from the uniaxial and the plane strain compression tests are shown in Fig. 9. In order for the slope to match at the origin, tensile stress was plotted as the measured values whereas the compressive stress (already scaled by 0.82) was further attenuated by $(1-\nu^2)$. The compressive strains plotted in Fig. 9 are the strains that were calculated from eqn (2). A Ramberg–Osgood fit is included in the tensile portion of the response for reference, and the material parameters are shown in Table 1. To assess the effect of friction in the compression tests, two different surfaces were considered. One was a dry surface, and the other lubricated with Vaseline. Both surface conditions yielded similar Young's moduli, which were found to be 1.96 GPa. This value was within 4% of the value from the uniaxial tension test (2.03 GPa). The inelastic response from both surface conditions gave rise to stress–strain curves that exhibited considerable decreases in slope (which never became negative) then followed by hardening. Similar behavior has been observed by Buisson and Ravi-Chandar (1990) in polycarbonate when stress and strain were extracted from local measurements during uniaxial tension experiments. The necking instability that was observed in the tension tests did not occur in the compression tests. The lubricated

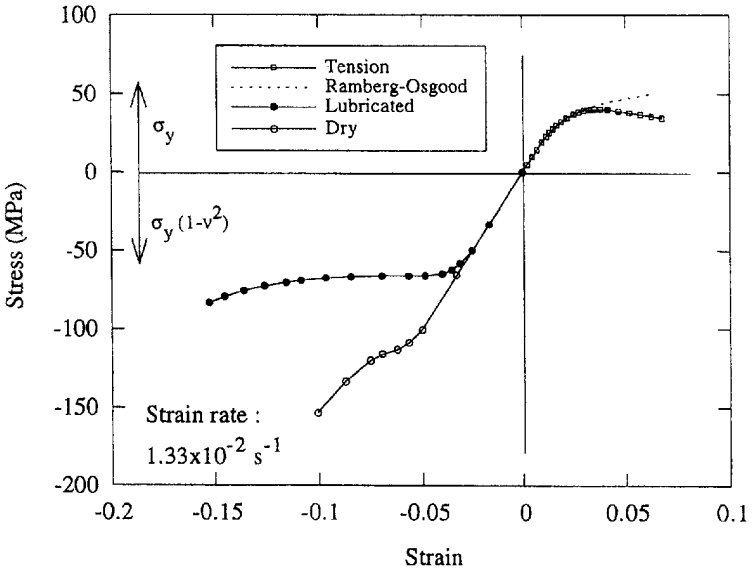

Fig. 9. Stress–strain responses in the plane strain compression and uniaxial tension tests.

Table 1. Material properties

Ramberg–Osgood representation

Material	Young's modulus E (GPa)	Poisson's ratio ν	Yield stress σ_0 (MPa)	Hardening exponent n	Yield offset $\tilde{\alpha}$
Epoxy	2.03	0.36	34.6	6	0.07

Yield stress comparison

Test method	σ_0(MPa)	τ_0(MPa)	$\dot{\varepsilon}$ (s^{-1})	$\dot{\gamma}$ (s^{-1})
Tension	34.6	20.0	0.50×10^{-3}	1.0×10^{-3}
Shear	31.5	18.2	0.125×10^{-3}	0.25×10^{-3}
Compression	76	43.9	1.25×10^{-3}	2.5×10^{-3}

Note: $\dot{\varepsilon} = \dot{\gamma}/2$, and $\tau_0 = \dfrac{\sigma_0}{\sqrt{3}}$ (von Mises criterion).

steel bars gave rise to a much longer plateau (to 10% strain) that occurred at a lower stress ($\sigma_y = 76$ MPa) than the level (126 MPa) that was produced by the dry steel bars. This difference was presumably due to the additional constraint provided by the dry bars. Finally, when the specimen was sectioned and viewed in crossed polars following removal from the plattens after unloading, there were no signs of shear banding, especially from the corners. The lack of any localization or softening in this experiment means that the nominal strain rate was the actual strain rate.

Plane strain compression testing has been used quite extensively for examining the post-yield behavior of polymers. The lack of softening in the epoxy being considered here is by no means universal and softening responses have been observed in some materials, although they have not always necessarily been the result of true material softening. In examining the plane strain compressive response of a number of different polymers, Williams (1967) found that polyvinyl chloride exhibited strain softening whereas others (high and low density polyethylene and acetal polymer) did not. Since the test does not suffer from any geometric effects in the sense that the measured stress is the true stress (in the absence of stress concentrations), the softening behavior was thought to be truly a material effect. Polystyrene and polymethylmethacrylate also exhibited a softening response, the degree of which became less severe (Bowden and Raha, 1970) with higher temperature and lower strain rates. However, it was found that shear bands formed in their experiments as

well as in those of Bowden and Jukes (1968, 1972) on polymethylmethacrylate, polyvinyl chloride, polyethylene terephthalate, polystyrene and a plasticized epoxy, all of which had exhibited softening behavior. In all cases, the shear bands initiated from stress concentrations at the corners of the compression dies, thus masking the possibility of true strain softening. Adam *et al.* (1975) also observed softening in polycarbonate under plane strain compression; annealing the material gave rise to a greater degree of softening but no mention was made of any attempts to detect shear banding.

Softening responses have also been attributed to strain rate effects. For example, G'Sell and Jonas (1979) found that softening in high density polyethylene under tension disappeared but still occurred in polyvinyl chloride when the experiments were conducted at constant strain rates rather than constant displacement rates. The lack of softening in high density polyethylene under tension at true constant strain rates is consistent with the results of the plane strain compression experiments of Williams (1967). In the recent experiments of Boyce *et al.* (1992) and Arruda and Boyce (1993a,c), where tests on polycarbonate and polymethylmethacrylate were conducted under truer plane strain conditions and constant strain rates, deformations were macroscopically homogeneous at all times but softening was still observed. The possibility of localization on a microscopic scale was acknowledged (Boyce *et al.*, 1992) and is certainly possible in view of recent work on propagating instabilities (Kyriakides, 1994) and the lack of softening in the tensile behavior of polycarbonate that was extracted by Buisson and Ravi-Chandar (1990) from local strain and birefringence measurements.

On the other hand, Knauss and Emri (1987) have shown, by including the effect of mechanical dilatation on free volume, that true material softening can indeed occur through the nonlinearity that is thereby introduced. This ties in with observations that annealing, which essentially reduces the free volume, caused increases in the degree of softening [see the review and discussion of various results by Haward (1980) and the recent positron annihilation lifetime spectrometry experiments of Hasan *et al.* (1993)]. The Knauss–Emri model has recently been extended to large strains by O'Dowd and Knauss (1992), with the introduction of a rubber elasticity component to account for orientational hardening. Finally, it is certainly possible that, as some of the experiments described above were being conducted (at higher strain rates), temperature rises occurred with concomitant softening, a situation that has recently been considered by Arruda *et al.* (1992) in a coupled thermomechanical analysis.

For the Arcan tests under pure shear at a displacement rate $\dot{\Delta} = 2.5$ μm/s, we have plotted the shear stress against the global shear strain and the shear strain at the specimen center (Fig. 10). The two measures of shear strain agreed closely up to the maximum load, at which time a shear band initiated along the centerline of the specimen due to the slightly higher stress levels there [Fig. 7(a)]. (In the shear specimen used by G'Sell (1986), shear banding was triggered by a small reduction in area at the center of the gage section.) Since the specimen was under displacement control, the overall load dropped sharply as a function of global shear strain. The drop-off with the central shear strain was not as marked because of the localization there. The material properties obtained from this test are also summarized in Table 1. The onset of localization occurred at $\tau_0 = 18.2$ MPa under pure shear. For the von Mises criterion, the yield stress under tension, σ_0, can be related to τ_0 by

$$\tau_0 = \frac{\sigma_0}{\sqrt{3}}. \tag{9}$$

The tensile yield stress σ_0 calculated from eqn (8) is 31.5 MPa, which is lower than the value from the tension test (34.6 MPa). The lower yield stress under pure shear was probably due to the fact that the applied strain rate (0.125×10^{-3}) was lower than that of the tension (0.5×10^{-3}) and the absence of hydrostatic stresses, as will be discussed later.

The moiré fringe data yield whole field information which was used to follow the development of the shear band. The first noticeable feature, which was apparent from direct observation of the grid even before moiré processing, was that the shear band seemed to

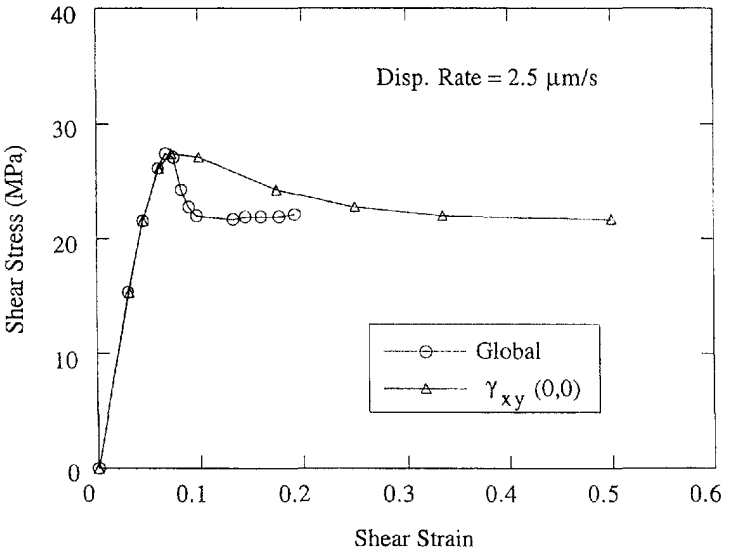

Fig. 10. Global and local responses in pure shear.

propagate essentially instantaneously in the y-direction. This initial observation was further quantified by extracting the shear strain from the moiré fringes across the gage section of the specimen along several y-locations (Fig. 11). A series of strain profiles are plotted at six load levels. The main feature of the plots is that there was no variation in shear strain with y-location. The profiles also exhibit the localization of the shear strain along the centerline ($x = 0$) of the specimen.

Since there was no y-dependence in the strain profiles, we will now focus more closely on the displacement and strain distributions along $y = 0$. The displacements are considered first in Fig. 12. At low applied displacement levels, the displacements were linear in (x/h), indicating simple shear across the gage section. At higher load levels, the displacement profiles became sigmoid, which suggested that localization was occurring. The displacement profiles were fitted (least square) by polynomial functions which were then differentiated to obtain the shear strains (Fig. 13). The onset of the localization can be seen clearly at the applied shear strain level (0.074) that corresponded to the maximum load. After that, the peak strain values increased as the shear band developed. In fact, the shear band also appeared to broaden or grow in the x-direction. This can be seen from the broadening of the region over which the normalized shear strain exceeded unity. The widening of the shear band suggested that the material in the middle of the band is stiffening, as noted by Wu and van der Giessen (1993) in their analysis of simple shear of polycarbonate and Fager and Bassani (1986) who considered neck propagation under plane strain tension.

The effect of strain rate on the global shear stress/strain response is shown in Fig. 14. The first effect of increasing the strain rate was to stiffen the response prior to the initiation of shear banding. This is expected from considerations of linearly viscoelastic response. Lowering the strain rate lowered the stress level at which shear banding initiated and increased the strain level at which specimen failure occurred. This is presumably due to the fact that the molecular rearrangements required for shear banding can occur more easily and extensively at the lower strain rates.

Increasing the amount of compression delayed the onset of shear banding (Fig. 15). The load drop following the initiation of a shear band was the same for all levels of compression. After the load drop, there was a slight increase in load instead of the plateau that was observed in the pure shear experiments. Increasing the degree of compression increased the strain at failure.

For $\alpha = -30^\circ$, displacement profiles along $y = 0$ were extracted from the moiré fringes at various load levels. The transition from linear to sigmoid distributions was again apparent (Fig. 4.12, Liang, 1993) and strains were extracted in the same manner as for the shear

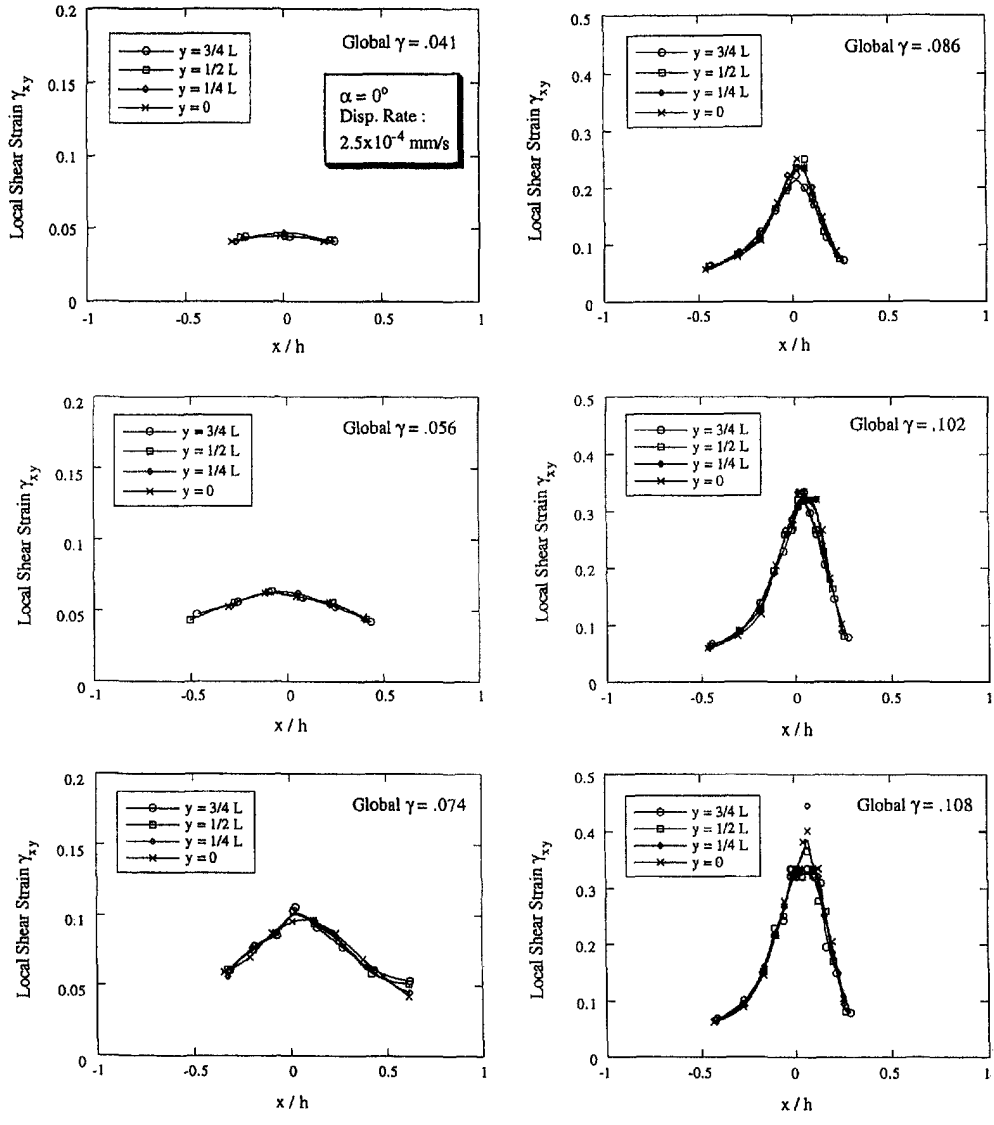

Fig. 11. Local shear strain distributions along the x-axis at various y-location.

experiments. The strains are shown in Fig. 16 and show more clearly than can be seen in Fig. 13 that the shear band was broadening as the applied displacement was increased.

A series of experiments was also conducted with increasing amounts of tension on shear. The global load/displacement response is shown in Fig. 17. Increasing the amount of tension first stiffened the initial response prior to the initiation of the shear banding. It also decreased the failure strains. The moiré fringe density was so low in these experiments that it was difficult to extract displacements. The use of higher frequency gratings was not pursued. The maximum stress levels, σ_0, corresponding to the initiation of shear bands for all the combinations of tension and compression on shear are shown in Fig. 18 as a function of the hydrostatic pressure. It can be seen that compression ($p > 0$) delayed the onset of shear banding whereas tensile stresses promoted it. This is consistent with the lack of shear banding and an accompanying load drop in the plane strain compression experiment (Fig. 9).

Some pure shear experiments were conducted with measurements of birefringence using a standard circular polarizer arrangement. The evolution of retardation with time is

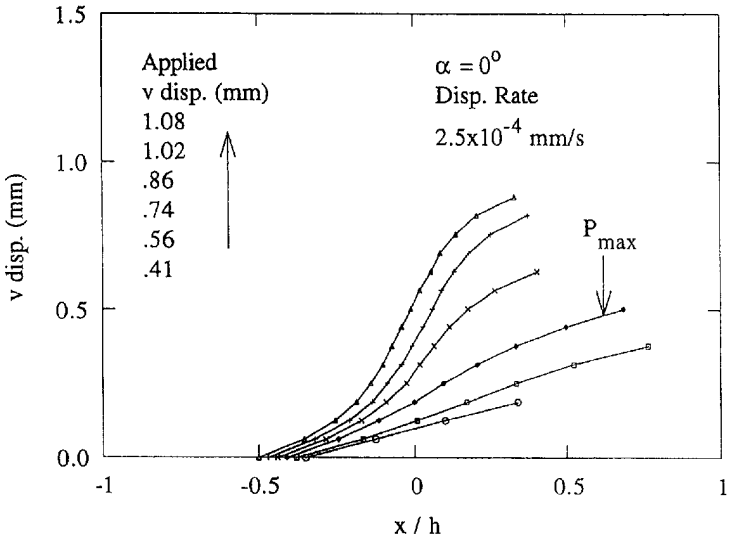

Fig. 12. Displacement fields along the x-axis under pure shear.

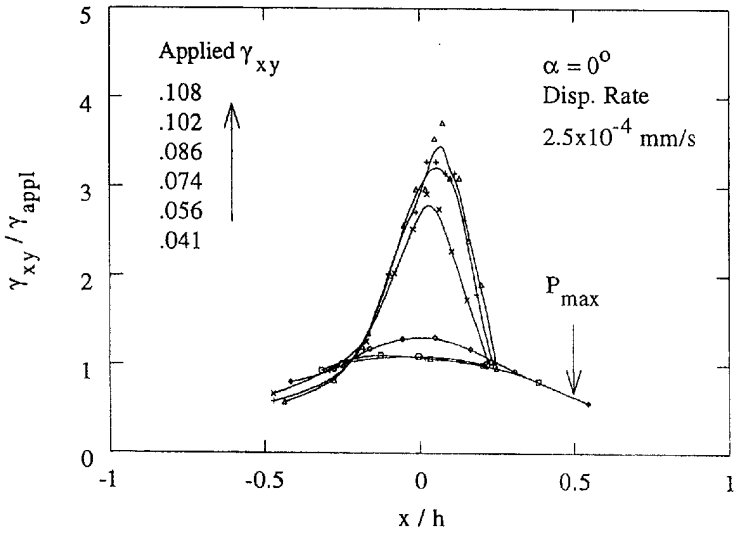

Fig. 13. Shear strain distribution during shear banding under pure shear.

shown in Fig. 19(a) along with that of the shear stress, the global shear strain and the local shear strain. Because the retardation and local strain could not be measured simultaneously in the same experiment, the local shear strain data was obtained from an experiment in which the load vs time response was essentially the same. The most striking feature of the various responses is that the retardation at the center of the specimen "locked up" or became constant as soon as the shear band initiated. The initiation of the shear band was marked by the limit load and the separation of the local and global shear strain responses. It is also interesting to note that the local shear strain at the specimen center eventually became constant as the broadening of the shear band became the dominant event. If we think of retardation being related to strains through eqn (6), then it is very surprising to see that, at the specimen center, the retardation became constant while the local shear strain was increasing. However, it is unlikely that (6) applies once shear banding has initiated and

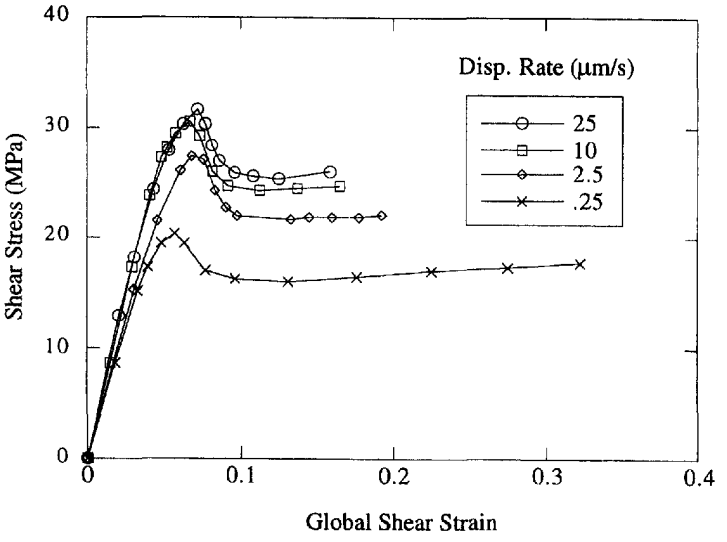

Fig. 14. Effect of strain rate under pure shear.

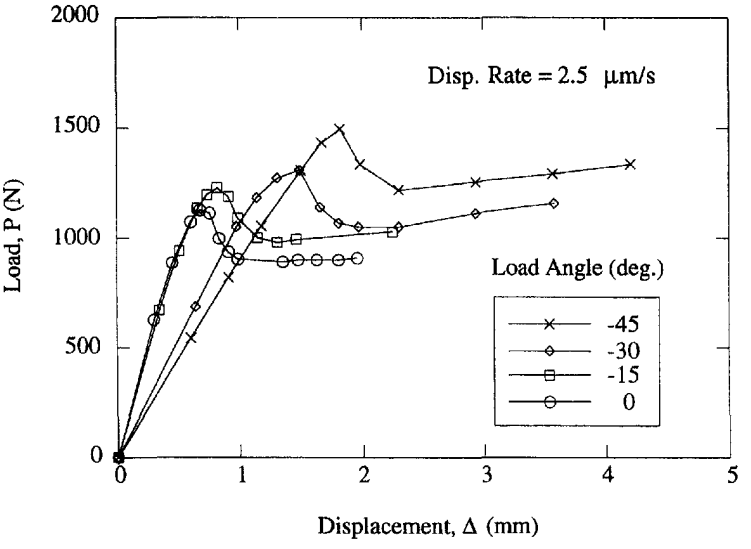

Fig. 15. Effect of compression superposed on shear.

the fact that the birefringence became constant suggests that, once orientation sets in a shear band, it remains the same. It should also be said that, although the retardation became constant at the specimen center, the fringe patterns continued to change outside what appeared to be the boundary of the shear band. This also suggests that there is a limit to the degree of anisotropy (molecular alignment) that can be reached.

The relationship between the shear stress and the retardation is shown in Fig. 19(b), which is a crossplot of the data in Fig. 19(a). The response was linear up to about the tenth fringe, which allowed f_σ to be extracted (eqn 7) from the slope as 4880 N/m (27.9 lb/in). The retardation due to the plastic strain, N^*, (up to shear band initiation) was then obtained by subtracting out the linear stress response so that, from eqn (8)

$$N^* = N - \frac{h\tau}{f_\sigma} = \frac{h}{2f_\varepsilon}\gamma^p. \tag{10}$$

The plot of N^* vs γ^p [Fig. 19(c)] deviated from the linearity suggested by eqn (8) for

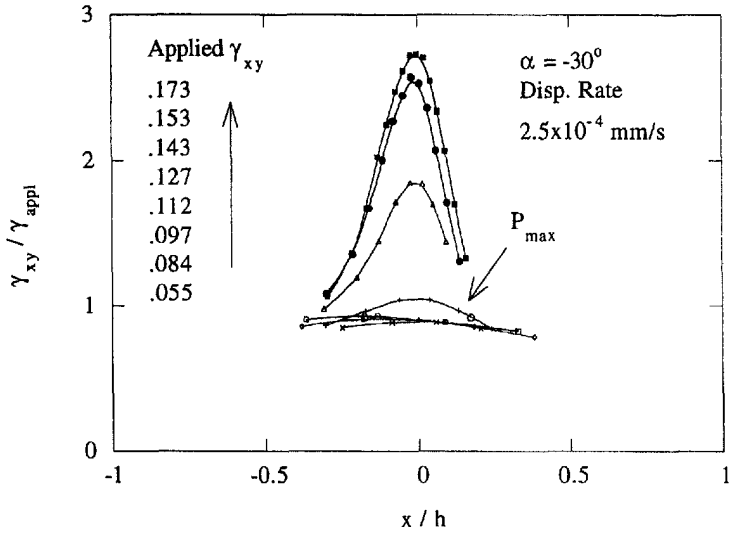

Fig. 16. Shear strain distribution during shear banding under compression and shear.

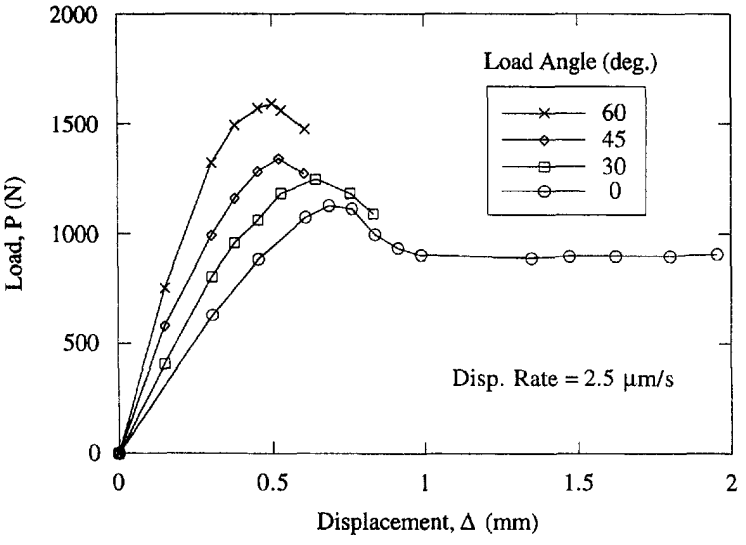

Fig. 17. Effect on tension superposed on shear.

$\gamma^{P} > 0.018$. The value of f_{σ} extracted from the slope of the linear portion of the response was 5.94×10^{-3} mm (2.34×10^{-4} in). However, the linearity of the response suggested by eqn (8) is clearly questionable for this material.

The softening that was observed in shear and the combinations of tension or compression on shear was associated with the initiation and propagation of a shear band. If we recall that, in the plane strain compression test, the epoxy did not exhibit any softening behavior and no shear banding was observed, then it is clear that the softening in the pure shear and biaxial experiments was geometric. However, this has to be weighed against the observation of Wu and van der Giessen (1993) that true material softening was needed to obtain shear banding. The observation was made as a result of considering a series of shear stress/strain curves with varying degrees of softening. Softening in nominal stress/stretch curves was also required to cause bulges to occur in pressurized polyethylene membranes (McGuire, 1993). At the same time, axisymmetric and plane strain neck propagation has been shown to occur in materials whose true stress/strain curves do not possess a maximum

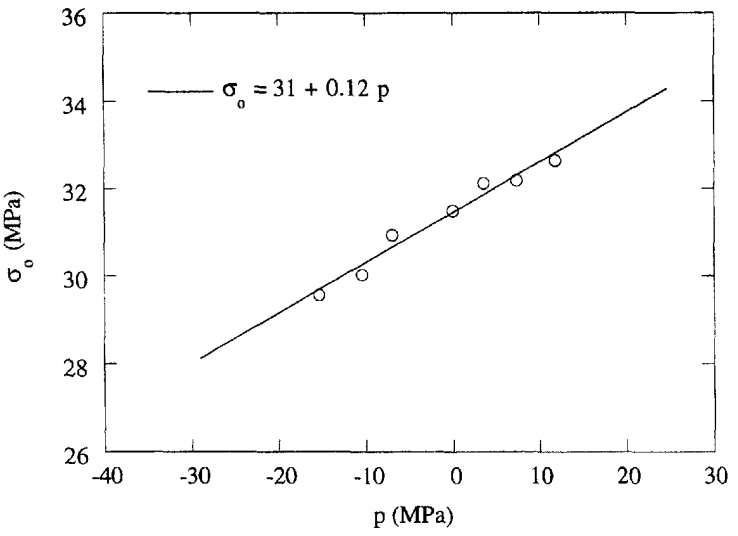

Fig. 18. Effect of hydrostatic pressure on the initiation of shear banding.

(Hutchinson and Neale, 1983; Neale and Tugcu, 1985; Fager and Bassani, 1986; Buisson and Ravi-Chandar, 1990).

In the Appendix, the data presented for tension and plane strain compression (Fig. 9), shear at various strain rates (Fig. 14), compression on shear (Fig. 15) and tension on shear (Fig. 17) was used to extract parameters for the Boyce, Parks, Argon (1988) model. The results are presented in Fig. 20, where a linear plot would indicate the validity of the model. Note that there is some curvature to the rather limited data set. Thus the parameters presented in Table 2 should be used with caution in any complementary computational efforts.

4. CONCLUSIONS

The deformation behavior of a bisphenol A epoxy hardened with an amido amine was examined using tensile, plane strain compression, and biaxial tests with combinations of tension or compression on shear. Arcan specimens were used to examine epoxy shear behavior at various strain rates and with various combinations of tension or compression. In the experiments with the Arcan specimen, measurements of the globally-controlled displacement and reactive load were complemented by measurements of birefringence and local displacements using geometric moiré. Localization occurred in the tensile, the pure shear and the biaxial experiments but not in the plane strain compression experiments. In the experiments with various amounts of shear, a single shear band first propagated longitudinally and then broadened laterally as has been noted on a number of occasions by G'Sell (1986) and G'Sell *et al.* (1990). The birefringence became constant with the initiation of the shear band. Although the onset of shear banding was delayed by higher strain rates and compressive stresses, it was promoted by tensile stresses. Parameters for the Boyce, Parks and Argon (1988) model were extracted from the plane strain compression (zero softening), simple shear (strain rate effects) and biaxial data (hydrostatic pressure effects) and form the basis for subsequent analysis. The detailed strain distributions in the shear bands should be useful for validating any analysis.

Acknowledgements—We would like to acknowledge the financial support provided by the Office of Naval Research and the National Science Foundation for this work through grant numbers N00014-90-J-4024 and MSS-9201929, respectively.

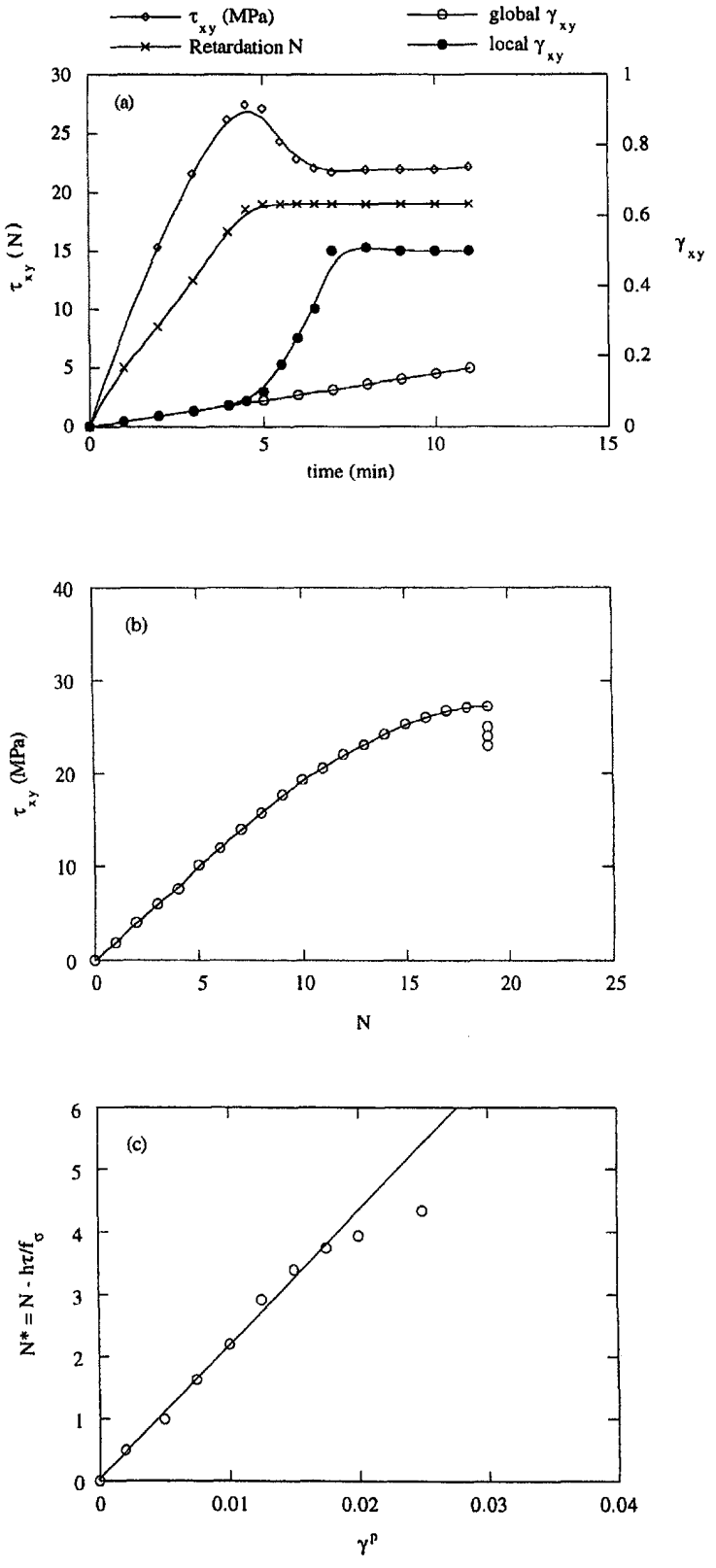

Fig. 19. Stress, strain, and retardation measurements in Arcan specimen under pure shear.

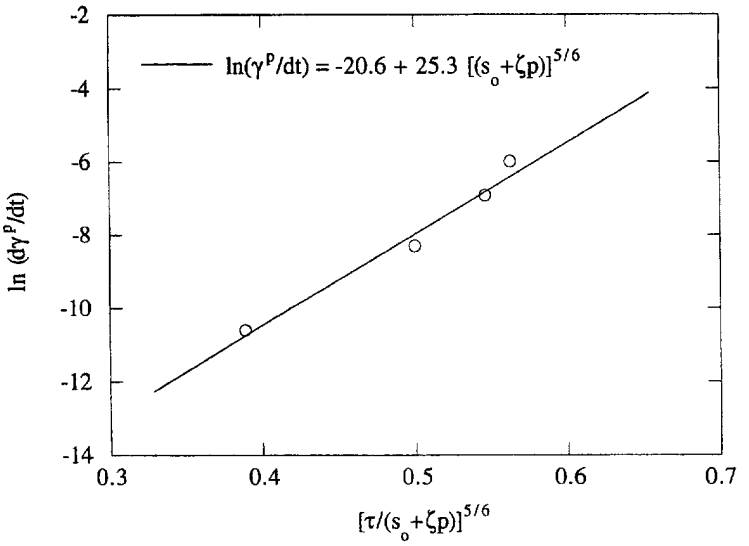

Fig. 20. Determination of the parameters in Argon's model.

Table 2. Material properties for the Boyce, Parks, Argon model

Initial athermal shear resistance s_0(MPa)	Pressure sensitivity coefficient ζ	Material constant A (K/MPa)	Pre-exponential shear strain rate factor $\dot{\gamma}_0$	Slope of yield drop h (MPa)
63.0	0.12	119	110	0

REFERENCES

Adam, G. A., Cross, A. and Haward, R. N. (1975). The effect of thermal pretreatment on the mechanical properties of polycarbonate. *J. Mater. Sci.* **10,** 1582–1590.

Arcan, M., Hashin, Z. and Voloshin, A. (1984). A method to produce uniform plane-stress states with applications to fiber-reinforced materials. *Exp. Mech.* **18,** 141–145.

Argon, A. S. (1973). A theory for the low-temperature plastic deformation of glassy polymers. *Phil. Mag.* **28,** 839–865.

Argon, A. S. and Bessonov, M. I. (1977). Plastic deformation in polyimides with new implications on the theory of plastic deformation of glassy polymers. *Phil. Mag.* **35,** 917–933.

Arruda, E. M., Boyce, M. C. and Jayachandran, R. (1995). Effects of strain rate, temperature and thermo-mechanical coupling on the finite strain deformation of glassy polymers. *Mech. Mater.* **19,** 193–212.

Arruda, E. M. and Boyce, M. C. (1993a). Evolution of plastic anisotropy in amorphous polymers during finite straining. *Int. J. Plasticity* **9,** 697–720.

Arruda, E. M. and Boyce, M. C. (1993b). A three dimensional constitutive model for the large stretch behavior of rubber elastic materials. *J. Mech. Phys. Solids* **41,** 389–412.

Arruda, E. M., Boyce, M. C. and Quintuz-Bosz, H. (1993c). Effects of initial anisotropy on the finite deformation behavior of glassy polymers. *Int. J. Plasticity* **9,** 783–811.

Bowden, P. B. and Jukes, J. A. (1968). The plastic yield behavior of polymethylmethacrylate. *J. Mater. Sci.* **7,** 183–190.

Bowden, P. B. and Raha, S. (1970). The formation of micro shear bands in polystyrene and polymethylmethacrylate. *Phil. Mag.* **22,** 463–482.

Bowden, P. B. and Jukes, J. A. (1972). The plastic flow of isotropic polymers. *J. Mater. Sci.* **7,** 52–63.

Boyce, M. C., Parks, D. M. and Argon, A. S. (1988). Large inelastic deformation of glassy polymers. Part I: rate dependent constitutive model. *Mech. Mater.* **7,** 15–33.

Boyce, M. C., Arruda, E. M. and Jayachandran, R. (1994). The large strain compression, tension and simple shear of polycarbonate. *Polymer Engng Sci.* **34,** 716–725.

Buisson, G. and Ravi-Chandar, K. (1990). On the constitutive behavior of polycarbonate under large deformation. *Polymer* **31,** 2071–2076.

Coker, E. G. and Filon, L. N. G. (1957). *A Treatise on Photoelasticity*. Cambridge University Press, Cambridge.

Fager, L. O. and Bassani, J. L. (1986). Plane strain neck propagation. *Int. J. Solids Structures* **22,** 1243–1257.

Ford, H. and Watts, A. B. (1952). An experimental investigation of the yielding of a strip between smooth dies. *Proc. Inst. Mech. Engrs* **1B,** 448.

G'Sell, C. (1986). Plastic deformation of glassy polymers: constitutive equations and macromolecular mechanisms. In *Strength of Metals and Alloys* (Edited by H. J. McQueen, J. P. Bailon, J. I. Dickson, J. J. Jonas and M. G. Akben), pp. 1943–1982. Pergamon Press, Oxford.

G'Sell, C. and Jonas, J. J. (1979). Determination of the plastic behavior of solid polymers at constant true strain rate. *J. Mater. Sci.* **14,** 583–591.

G'Sell, C., Jaques, D. and Favre, J. P. (1990). Plastic behavior under simple shear of thermosetting resins for fiber composite matrices. *J. Mater. Sci.* **25,** 2004–2010.
Hutchinson, J. W. and Neale, K. W. (1983). Neck propagation. *J. Mech. Phys. Solids* **31,** 405–426.
Hasan, O. A., Boyce, M. C., Li, X. S. and Berko, S. (1993). An investigation of the yield and postyield behavior and corresponding structure of polymethylmethacrylate. *J. Polymer Sci. Part B: Polymer Phys.* **31,** 185–197.
Haward, R. N. (1980). The effect of chain structure on the annealing and deformation behavior of polymers. *Colloid Polymer Sci.* **258,** 643–662.
Knauss, W. G. and Emri, I. (1987). Volume change and the nonlinearly thermo-viscoelastic constitution of polymers. *Polymer Engng Sci.* **27,** 86–101.
Kyriakides, S. (1994). Propagating instabilities in structures. *Adv. Appl. Mech.* **30,** 67–189.
Lee, S. M. (1988). Plastic deformation in epoxy resin. In *Cross-linked Polymers: Chemistry, Properties, and Application* (ACS symposium series no. 367, Edited by R. A. Dickie, S. S. Labana and R. Bauer), pp. 136–144. American Chemical Society, Washington, DC.
Liang, Y.-M. (1993). Toughening mechanisms in mixed-mode interfacial fracture. Ph.D. Dissertation, The University of Texas at Austin.
Liang, Y.-M. and Liechti, K. M. (1995) Toughening mechanisms in mixed-mode interfacial fracture. *Int. J. Solids Structures* **32,** 957–978.
Liechti, K. M. and Liang, Y.-M. (1992). The interfacial fracture characteristics of bimaterial and sandwich blister specimens. *Int. J. Fracture* **55,** 95–114.
McGuire, M. K. (1993). Localization in high-density polyethylene structures. MS Thesis, The University of Texas at Austin.
Neale, K. W. and Tugcu, P. (1985). Analysis of necking and neck propagation in polymeric materials. *J. Mech. Phys. Solids* **33,** 323–337.
O'Dowd, N. and Knauss, W. G. (1992). Time-dependent, large deformation of polymers. GALCIT SM 92-40, California Institute of Technology Technical Report.
Raha, S. and Bowden, P. B. (1972). Birefringence of plastically deformed poly(methylmethacrylate). *Polymer* **13,** 174–183.
Treloar, L. R. G. (1958). Chapter V in *Physics of Rubber Elasticity*. Oxford University Press, Oxford.
Williams, J. G. and Ford, H. (1964). Stress–strain relationships for some unreinforced plastics. *J. Mech. Engng Sci.* **6,** 405–417.
Williams, J. G. (1967). Stress–strain compression testing of polymers. *Trans. J. Plastics Inst.* **35,** 505–508.
Wu, P. D. and van der Giessen, E. (1992). A modified 3-D constitutive model for glassy polymers and its application to large simple shear of polycarbonate. In *Modelling of Plastic Deformation and its Engineering Applications* (Edited by S. I. Andersen, J. B. Bilde-Sörensen, N. Hansen, D. Juul Jensen, T. Leffers, H. Lilholt, T. Lorentzen, O. B. Pedersen and B. Ralph), pp. 519–524. Roskilde, Denmark.
Wu, P. D. and van der Giessen, E. (1993). Analysis of shear band propagation in amorphous glassy polymers. Delft University of Technology Report no. 1014. *Int. J. Solids Structures* **31,** 1493–1517.
Yamini, S. and Young, R. J. (1980). The mechanical properties of epoxy resin. Part I: mechanisms of plastic deformation. *J. Mater. Sci.* **15,** 1814–1822.

APPENDIX

Determination of parameters for the Boyce, Parks Argon model

The data presented in Figs 9, 14, 15 and 17 has been used to identify the parameters in the models of yielding of thermoplastics that were proposed by Argon and Bessonov (1977) and Boyce *et al.* (1988). The constitutive law in these models accounts for the large, inelastic deformation behavior of glassy polymers. At temperatures below the glass transition temperature, plastic flow and the subsequent molecular chain alignment are resisted by the neighboring chains. The double-kink model of the intermolecular resistance proposed by Argon and Bessonov (1977) was generalized for three dimensional behavior in the paper by Boyce *et al.* (1988) in order to account for inelastic deformation that exhibits strain rate, temperature and pressure dependent yield, as well as strain softening and hardening after yield. A total of five material properties were identified by several testing procedures.

The rate of plastic straining can be expressed as

$$\dot{\gamma}^{p} = \dot{\gamma}_0 \exp\left[-\frac{A\tilde{s}}{\Theta}\left(1-\left(\frac{\tau}{\tilde{s}}\right)^{5/6}\right)\right] \tag{A1}$$

where $\dot{\gamma}_0$ and A are material constants, Θ is the absolute temperature, τ is the applied shear stress, and $\tilde{s}$, the effective athermal shear resistance, is defined through

$$\tilde{s} = s + \zeta p \tag{A2}$$

where s is the current athermal deformation resistance of the material indicating the current state of the structure, p is the hydrostatic pressure, and ζ is the pressure sensitivity coefficient. The initial value of the athermal resistance is

$$s_0 = 0.077\frac{\mu}{1-\nu} \tag{A3}$$

where μ and ν are shear modulus and Poisson's ratio respectively. The evolution equation for the athermal shear resistance is

$$\dot{s} = h\left(1 - \frac{s}{s_{ss}(\Theta, \dot{\gamma}^p)}\right)\dot{\gamma}^p \tag{A4}$$

where h is a material constant, and s_{ss} can be found from material softening test data.

The initial athermal shear resistance s_0 was obtained from eqn (A3) by using the shear modulus and Poisson's ratio measured at room temperature (25°C). The pressure sensitivity coefficient ζ in eqn (A2) was the slope of the yield stress vs hydrostatic pressure plot (Fig. 18). In order to find the material constant A and the pre-exponential shear strain rate factor $\dot{\gamma}_0$ in eqn (A1), it is convenient to write the equation as

$$\ln \dot{\gamma}_p = B + C\left(\frac{\tau}{s_0 + \zeta p}\right)^{5/6} \tag{A5}$$

where B and C are the intercept and slope, respectively, in a $\ln \dot{\gamma}_p$ vs $[\tau/(s_0+\zeta p)]^{5/6}$ plot (Fig. 20), where the data was obtained from the pure shear experiments at various rates (Fig. 14). The constants A and $\dot{\gamma}_0$ can then be determined through $A = C\Theta/(s_0+\zeta p)$ and $\dot{\gamma}_0 = \exp(B+C)$. As discussed earlier, there was no strain softening in the plane strain compression experiment (Fig. 9) so that the softening parameter h in eqn (A4) was zero. Furthermore, the amount of softening represented by $(\sigma_{max}-\sigma_{min})/\sigma_{max}$ in Fig. 14 was not very sensitive to strain rate. As a result, the quantity s_{ss} in eqn (A4) was taken to be a function of temperature only. However, for temperatures below the glass transition, the softening is also insensitive to temperature (Boyce *et al.*, 1988), so, s_{ss} was taken to be constant. The ratio s_{ss}/s_0 was taken be 1.0 for the epoxy. The values of the five material constants determined above are summarized in Table 2. Note that the data in Fig. 20 is quite limited and does not provide a complete check on the validity of the Boyce, Parks, Argon model.